

Journal of Materials Chemistry A

Accepted Manuscript



This is an *Accepted Manuscript*, which has been through the Royal Society of Chemistry peer review process and has been accepted for publication.

Accepted Manuscripts are published online shortly after acceptance, before technical editing, formatting and proof reading. Using this free service, authors can make their results available to the community, in citable form, before we publish the edited article. We will replace this *Accepted Manuscript* with the edited and formatted *Advance Article* as soon as it is available.

You can find more information about *Accepted Manuscripts* in the [Information for Authors](#).

Please note that technical editing may introduce minor changes to the text and/or graphics, which may alter content. The journal's standard [Terms & Conditions](#) and the [Ethical guidelines](#) still apply. In no event shall the Royal Society of Chemistry be held responsible for any errors or omissions in this *Accepted Manuscript* or any consequences arising from the use of any information it contains.

Carbon Nanotube@Layered Nickel Silicate Coaxial Nanocables as Excellent Anode Materials for Lithium and Sodium Storage

Chen-Xi Gui, Shu-Meng Hao, Yuan Liu, Jin Qu*, Cheng Yang, Yunhua Yu, Qian-Qian Wang and Zhong-Zhen Yu*

5 Received (in XXX, XXX) Xth XXXXXXXXXX 20XX, Accepted Xth XXXXXXXXXX 20XX

DOI: 10.1039/b000000x

Layered nickel silicate provides massive interlayer space that is similar to graphite for the insertion and extraction of lithium ions and sodium ions; however, the poor electrical conductivity limits its electrochemical application in energy storage devices. Herein, carbon nanotube@layered nickel silicate
10 (CNT@NiSiOx) coaxial nanocables with flexible nickel silicate nanosheets grown on conductive carbon nanotubes (CNTs) are synthesized with a mild hydrothermal method. CNTs serve as the conductive cables to improve the electron transfer performance of nickel silicate nanosheets, resulting in reduced contact and charge-transfer resistances. In addition to high specific surface area, short ion diffusion distance and good electrical conductivity, the one-dimensional coaxial nanocables have a stable structure
15 to sustain volume change and avoid structure destruction during the charge/discharge process. As an anode material for lithium storage, the first cycle charge capacity of the CNT@NiSiOx nanocables reaches 770 mA h/g with the first cycle Coulombic efficiency as high as 71.5 %. Even after 50 cycles, the charge capacity still reaches 489 mA h/g at a current density of 50 mA/g, which is nearly 87 % and 360 %
20 higher than those of NiSi/CNT mixture and nickel silicate nanotube, respectively. As anode material for sodium storage, the coaxial nanocables exhibit a high initial charge capacity of 576 mA h/g, which even retains 213 mA h/g at 20 mA/g after 16 cycles.

Introduction

Energy shortage is one of the most serious social issues today. Among all energy storage devices, rechargeable batteries such as
25 lithium-ion batteries (LIBs) and sodium-ion batteries (SIBs) have become the major types of energy supply devices for portable electronic devices because of their high energy density, long lifespan, wide temperature range and lightweight.¹⁻⁶ The performances of LIBs and SIBs largely depend on the electrodes
30 and electrolyte. Ideal anodes must meet the following requirements: good electronic and ionic conductivity, insolubility in the electrolyte, stable potential close to that of lithium/sodium metal, low molecular weight, cost-effective and environmentally benign.⁷⁻⁹ The researches on LIBs anode materials have
35 developed from Li metal and Li alloy to carbon materials, metal oxides, and Sn- or Si-based anode materials, etc.¹⁰⁻¹⁷ Graphite is the most common commercialized material for LIBs anode because of its stable performance and low cost. However, its low specific capacity (372 mA h/g) limits its energy density.
40 Meanwhile, it is not suitable for the intercalation of sodium ions because of the small interlayer spacing.^{18, 19} Therefore, it is highly imperative to find alternative anode materials.²⁰⁻²⁵

Silicate nanomaterials have been widely used in adsorption,<sup>26-
30</sup> catalyst^{31, 32} and drug delivery^{33, 34} because of their simple

45 preparation, rich source, low cost and unique porous structure. They are also promising candidates for LIBs/SIBs because they exhibit a similar charge/discharge behaviour with graphite and their tuned layered structure could provide ion transport routes.<sup>35-
39</sup> For example, Yang et al. prepared magnetic multi-walled
50 nickel silicate nanotubes by self-curling effect of layered structure.³⁶ The layered structure was very stable and the interlayer spacing remained almost unchanged during the charge/discharge cycles. Although the first cycle discharge capacity was 1523 mA h/g, the reversible capacity was only 227
55 mA h/g after 20 cycles. Yang et al. synthesized a flower-like nickel oxide/nickel silicate nanocomposite with a high first cycle discharge capacity of 1440 mA h/g,³⁸ but its reversible capacity reduced to 126 mA h/g only after 50 cycles. Although layered
60 silicate nanomaterials have the advantage of stable structure, their poor electrical conductivity is responsible for the large irreversible capacity. A second phase with good electron transfer effect is expected to enhance the electrochemical performance of layered silicate materials as LIBs/SIBs anodes. We enhanced the
65 anode performance of layered zinc silicates by introducing interlayer carbon and reduced graphene oxide into the system.³⁷ By adjusting the amount of carbon precursor, the interlayer spacing could be altered between 1.22 to 3.37 nm, the specific capacity increased from 232 mA h/g for neat zinc silicate, to 455 mA h/g for zinc silicate/interlayer carbon composite, and further

to 778 mA h/g for the composite with reduced graphene oxide. This indicates that carbonaceous materials could be efficient additives to layered silicates as anode materials. Carbon nanotubes (CNTs) not only serve as the conducting component due to their high electrical conductivity, but also they function as an active component for the intercalation of lithium ions.⁴⁰⁻⁴² CNTs have already been introduced into various nanostructures, including Si, Sn, Fe₃O₄, MnO₂, MoS₂, TiO₂ and SnO₂.⁴³⁻⁵⁴ These materials exhibit improved specific capacity and better electrochemical performance after the incorporation of CNTs.

Herein, we designed carbon nanotube@layered nickel silicate (CNT@NiSiOx) coaxial nanocables with nickel silicate (NiSiOx) nanosheets covalently bonded to CNTs to improve the electrical conductivity of layered nickel silicates. The coaxial nanocables are fabricated using CNT as the hard template as well as conducting network. Layered nickel silicates with an interlayer distance of 0.74 nm provide massive interlayer space for the insertion and extraction of lithium ions or sodium ions. Meanwhile, the tubular structure also serves as the structure buffer, preventing structural damage during charge/discharge processes, which ensures the performance stability during functioning. Thus, CNT@NiSiOx coaxial nanocables show an excellent lithium-ion storage performance with the first cycle Coulombic efficiency as high as 71.5 % and specific capacity of 489 mA h/g at a rate of 50 mA/g after 50 cycles, much higher than those of NiSi/CNT mixture (261 mA h/g) and nickel silicate nanotube (NiSNT) alone (107 mA h/g). Even for sodium-ion storage, the CNT@NiSiOx coaxial nanocables exhibit a high initial charge capacity of 576 mA h/g.

Experimental Section

Materials. Multi-walled CNTs were purchased from Shenzhen Nanotech Port Co. (China) with an average diameter of 40-60 nm, and CNTs were acid treated before delivery. Sodium hydroxide (NaOH, 1mol/L) and ammonium hydroxide (NH₃ H₂O, 28%) were bought from Beijing Chemical Factory (China). Nickel(II) chloride hexahydrate (NiCl₂ 6H₂O), ammonium chloride, tetraethyl orthosilicate (TEOS) and cetyl trimethyl ammonium bromide (CTAB) were supplied by Sinopharm Chemical Reagent Co. (China). All chemicals are analytical grade and were used without further purification.

Synthesis of CNT@silica nanotubes (CNT@SNTs). CNT@SNTs were prepared by sol-gel method. CNT (0.15 g) and CTAB (0.62 g) were ultrasonicated in 100 mL ethanol and 150 mL deionized water for 6 h. NaOH solution (300 mL) was then added dropwise, followed by stirring for 30 min. After 1.2 mL TEOS was added, the suspension was stirred for 8 h. Finally, the product was centrifuged and washed with ethanol for several times before drying at 60 °C for 12 h.

Synthesis of CNT@NiSiOx nanocables. CNT@NiSiOx nanocables were prepared using a hydrothermal method. CNT@SNT (50 mg) were dispersed in 20 mL deionized water by ultrasonication for 2 h to be Suspension A. Nickel chloride hexahydrate (178.27 mg), ammonium chloride (530.5 mg) and NH₃ H₂O (1 mL) were dissolved in 30 mL deionized water to be Solution B. Suspension A and Solution B were mixed and transferred to a 100 mL autoclave at 90 °C for 10 h. The product was centrifuged, rinsed with deionized water for several

times, and finally dried in an oven at 60 °C for 12 h.

Synthesis of NiSNTs. Black CNT@SNTs were heated in a muffle furnace at 550 °C for 7 h to burn off the CNT component and thus obtain white silica nanotubes. The rest synthesis route for NiSNTs is similar to that of CNT@NiSiOx nanocables.

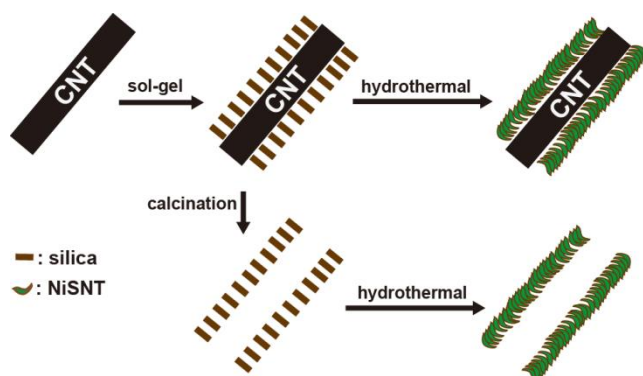
Characterization. X-ray diffraction (XRD) measurement was carried out using a Rigaku D/Max 2500 diffractometer with CuK α radiation ($\lambda=1.54$ Å) at a generator voltage of 40 kV and a generator current of 40 mA. CNT@nickel silicate and neat nickel silicate were characterized with a Thermo VG RSCAKAB 250X high-resolution X-ray photoelectron spectroscopy (XPS) and a Renishaw inVia Raman microscope (Britain). Fourier-transform infrared spectroscopy (FT-IR) was recorded using a Nicolet Nexus 670 FTIR spectrophotometer. The morphology and microstructure were observed with a Hitachi S4700 field-emission scanning electron microscope (SEM) and JEOL JEM-3010 transmission electron microscope (TEM). Thermogravimetric analysis (TGA) measurements were carried out using a TA Instruments Q50 thermogravimetric analyzer at a heating rate of 10 °C/min in air atmosphere. Brunauer-Emmett-Teller (BET) method was used to measure specific surface areas using N₂ adsorption and desorption isotherms on an Autosorb-1 analyzer at 78.3 K.

Electrochemical Measurements. Electrochemical tests were performed using coin-type cells assembled in an argon-filled glove box. The working electrode was composed of 70 wt% active material, 20 wt% super-P and 10 wt% polyvinylidene fluoride. For lithium ions battery application, the electrode slurry was cast onto nickel foam. The electrolyte was from Tianjin Jinniu Power Sources Material Co. Ltd. (China) and it was prepared by dissolving 1 M LiPF₆ in a mixture of ethylene carbonate, dimethyl carbonate, and diethyl carbonate with a weight ratio of 1:1:1. Lithium foil was used as the counter electrode. Mesoporous polyethylene/polypropylene membrane was used as the separator. Galvanostatic charge-discharge curves and cycling performance were measured with a Land CT 2001A electrochemical workstation at current densities of 50-1000 mA/g and voltage range from 0.01 to 3.0 V (vs. Li⁺/Li). Cyclic voltammograms (CV) and electrochemical impedance spectroscopy (EIS) were recorded on Metrohm Autolab PGSTAT 302N electrochemical workstation. CV was measured at a scanning rate of 0.1 mV/s within the voltage window of 0.01-3.0 V. For EIS measurement, the AC modulation amplitude is 10 mV and the frequency range is 10 kHz- 0.1 Hz. For sodium ions battery application, the above slurry was cast on copper foil and dried to obtain working electrode. Neat Na foil was used as the counter electrode. Whatman GF/D glass fiber was used as the separator membrane. The electrolyte consists of 1M NaPF₆ in the mixture of propylene carbonate/ethylene carbonate with a volume ratio of 1:1. The cells were galvanostatically cycled by the Land CT 2001A electrochemical workstation at voltages of 0.01 to 2.70 V (vs. Na⁺ /Na).

Results and discussion

Scheme 1 describes the two-step programmed preparation procedure of CNT@NiSiOx nanocables using dual templating method. CNT is used as the hard template as well as the conducting core; CTAB is adsorbed on the surface of CNTs and

served as the soft template. Silica layer is precisely coated on the surface of CNTs by the hydrolysis of TEOS in the alkaline condition. Then, nickel silicate nanosheets are formed around CNT by the in situ reaction of silica with nickel ions during the hydrothermal treatment at the mild condition of 90 °C, and the core-shell CNT@NiSiOx nanocables are formed. There are several advantages of this synthesis strategy: first, we used a much milder fabrication temperature of 90 °C, which is below water boiling point and allows the material to be fabricated in an open system instead of the reported closed autoclave or glass bottle;^{36, 55} second, this current strategy is general applicable and could also be used for the synthesis of other CNT-based nanocables, as reported in our work before;²⁷ third, this simple synthesize process is beneficial for the large scale production of CNT-based nanocables, which increases its potential for practical usage. For comparison, by burning off the CNT component, neat silica nanotubes are left. NiSNTs are also formed by a similar hydrothermal treatment.



Scheme 1. Schematic of the synthesis process of CNT@NiSiOx and NiSNT.

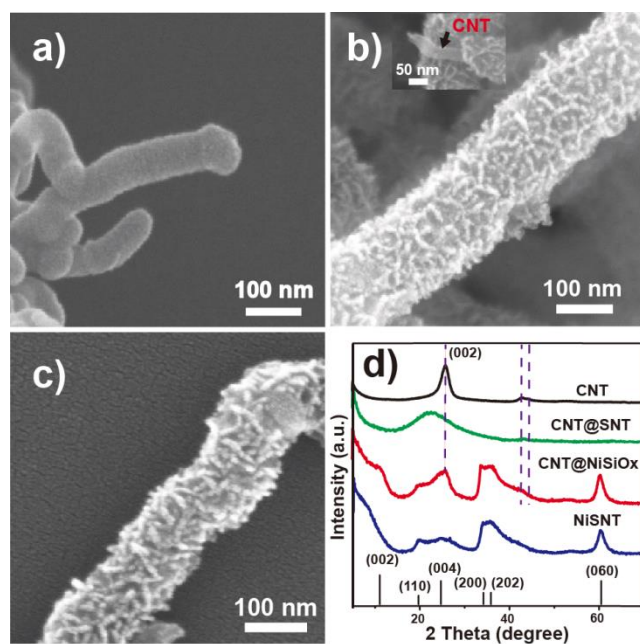


Figure 1. SEM images of a) CNT@SNT, b) CNT@NiSiOx, and c) NiSNT; d) XRD patterns of CNT, CNT@SNT, CNT@NiSiOx and NiSNT. Inset: broken edge of CNT@NiSiOx shows the inner CNT core.

Figure 1 reveals the morphology and crystallographic information of CNT@SNT, CNT@NiSiOx and NiSNT. Compared to the smooth surface of CNT (Figure S1), CNT@SNT exhibits a rougher surface due to the silica layer on CNT (Figure 1a). Figure 1b clearly shows the coaxial structure with NiSiOx nanosheets well dispersed and attached on CNT. For neat NiSNT, NiSiOx nanosheets are also assembled in similar one-dimension morphology (Figure 1c). EDX elemental mapping shows the distributions of Ni, Si, O and C in CNT@NiSiOx (Figure S2). In their XRD patterns (Figure 1d), all peaks of CNT@NiSiOx could be index to Ni₃Si₂O₅(OH)₄ (JCPDS no.49-1859). No other impurities are observed. The wide peak around 12° confirms its layered structure, corresponding to a d-spacing of 0.74 nm (Figure 1d and Figure S3). The layered structure will be characterized further later. The characteristic (002) peak of CNT is clearly observed in CNT@NiSiOx but it is not predominant in NiSNT, suggesting the absence of CNT in NiSNT. EDS

To investigate the formation process of CNT@NiSi, time-dependent experiments are carried out. Figure S4 shows different morphologies of CNT@NiSiOx and NiSNT after reaction for 0.5, 1 and 3 h. In the first hour, large amount of small granules and wrinkles are observed on the surface of CNT@SNT, indicating the dissolution of silica under alkaline condition. After the reaction for 3 h, silicate ions begin to react with nickel ions and form plate-like NiSiOx on CNT until all CNT are covered with NiSiOx nanosheets, and the regularity of the nanosheets increases with the reaction time.

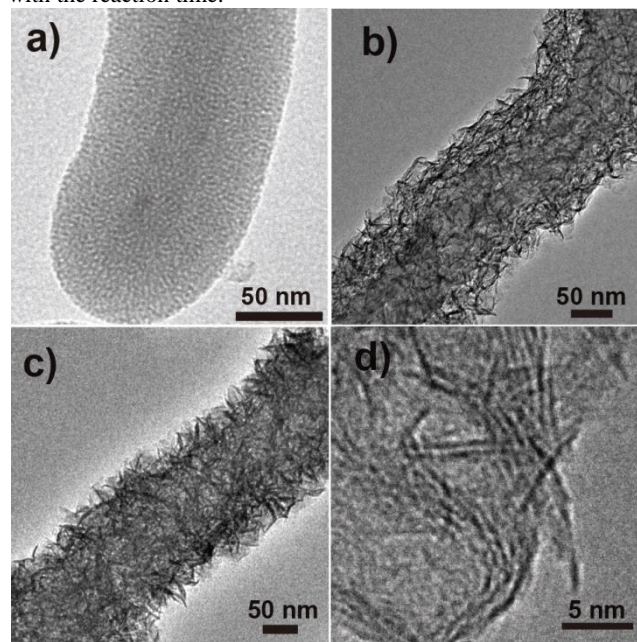


Figure 2. TEM images of a) CNT@SNT, b) CNT@NiSiOx, c) NiSNT; d) HRTEM image of NiSiOx nanosheets.

TEM images of CNT@SNT, CNT@NiSiOx and NiSNT clearly show the coaxial structural (Figure 2). The thickness of silica coating in CNT@SNT is evenly distributed and is almost the same as the diameter of CNT (~40 nm). After hydrothermal process, the twisted NiSiOx nanosheets form a porous layer around CNT, and the diameter of CNT@NiSiOx is increased to ~160 nm (Figure 2b). The contrast between the core and the surface confirms the core-shell structure. In the absence of CNT,

NiSNT exhibits a hollow structure (Figure 2c). Lamellar structure of the synthesized NiSiOx on CNT is confirmed by HRTEM (Figure 2d) with an interlayer spacing of ~0.74 nm, which agrees well with its XRD result. The spacing of 0.74 nm between the layers is much larger than Li⁺ and Na⁺, and such an analogous structure to graphite is proposed as competitive candidate for anode materials in lithium-ion or sodium-ion storage.

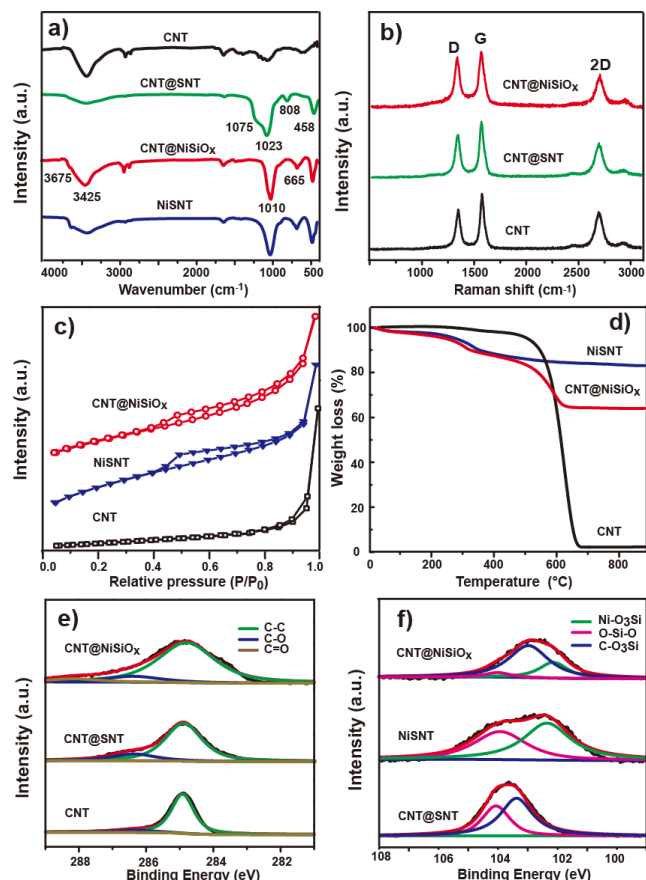


Figure 3. a) FTIR spectra of CNT, CNT@SNT, CNT@NiSiOx and NiSNT; b) Raman spectra of CNT, CNT@SNT and CNT@NiSiOx; c) N₂ adsorption/desorption isotherms; d) TGA curves of CNT, CNT@NiSiOx and NiSNT; e) C 1s and f) Si 2p XPS spectra of CNT, CNT@SNT, CNT@NiSiOx and NiSNT.

Figure 3a shows FT-IR spectra of CNT@NiSiOx, CNT@SNT, NiSNT and CNT. The peaks around 2852 cm⁻¹ are related to the stretching vibration of C-H and the peak at 1629 cm⁻¹ is associated with C=O or the deformation vibration of physically adsorbed water. The broad band at 3425 cm⁻¹ corresponds to the hydrogen-bonded hydroxyl groups of adsorbed water molecules; while the narrow peak at 3675 cm⁻¹ is related to the Ni-OH stretching mode,^{56,57} similar phenomenon could also be observed in magnesium silicates.^{58,59} In silica sample, two strong adsorption peaks at 1075 cm⁻¹ and 1023 cm⁻¹ are ascribed to the longitudinal-optical and transverse-optical modes of asymmetric Si-O-Si bond stretching vibrations, and the peak at 808 cm⁻¹ is from symmetrical Si-O-Si network bond stretching vibrations.⁶⁰ However, in the FT-IR pattern of nickel silicate, the adsorption peaks at 1075 cm⁻¹ and 808 cm⁻¹ disappear, and the peak at 1023 cm⁻¹ shifts to 1010 cm⁻¹, which may be ascribed to the formation of Si-O-Ni bonds. In addition, a new absorption peak at about

665 cm⁻¹ is associated with lattice vibration of nickel-oxygen bonds in the nickel silicate sample.^{59, 61}

Raman is used to investigate the structural change of CNT@NiSiOx (Figure 3b). The D band at ~1340 cm⁻¹ and the G band at ~1590 cm⁻¹ are two most distinctive bands of graphitic carbon network. It is commonly agreed that G band is related to the first-order scattering of the E_{2g} mode for sp² carbon domains, while D band represents structural defects or edges that break the symmetry and selection rule. The intensity ratio of the D band to the G band (I_D/I_G) is usually used to measure the graphitization degree of carbon materials. The I_D/I_G value of CNT is 0.72; after coated with silica, it increases to 0.77, and then, the value further increases to 0.91 for CNT@NiSiOx, indicating that more defects are introduced to the carbon network by coating with silica and NiSiOx, and these defects could also serve as storage sites for lithium ions.⁶²

XPS surveys (Figure S5) further prove the formation of NiSiOx. Figure 3e confirm that such a sol-gel and hydrothermal treatment slightly damages sp² carbon domain and induces the formation of oxygen-containing functional groups, which would contribute to the covalent bonding between NiSiOx nanosheets and CNT. Curve fitting results of Si 2p supports our hypothesis (Figure 3f). The basic structure of Ni₃Si₂O₅(OH)₄ composes of a three-layer sheet with a layer of silicon-oxygen tetrahedron sharing oxygen atoms at the corner, two layers of nickel/hydroxide ions connected to silicon-oxygen layer by Van der Waals forces.²⁶⁻³⁰ The peaks at 103.9 and 102.2 eV are assigned to silicon-oxygen tetrahedron layer and the bonds between nickel/hydroxide ions with silicon-oxygen layer. Thus, the peak at 103.0 eV should be ascribed to the strong C-O-Si covalent bond between CNT and NiSiOx nanosheets. The covalent bond provides tight binding between CNT and NiSiOx, which ensures the structure integrity during the cycling process and thus the cycling stability of the composite. In addition, the oxygen bridge between CNT and NiSiOx leads to the charge overlap in the interface and thus forms a good pathway for the electron transfer during charge-discharge cycles.⁶³⁻⁶⁵

The specific surface areas of CNT, CNT@NiSiOx and NiSNT are obtained from N₂ adsorption and desorption isotherms (Figure 3c). The isotherms of CNT@NiSiOx and NiSNT are similar to each other but quite different from that of CNT, and both of them could be classified as type IV, a typical shape of mesoporous material. The BET specific surface area is 62 m²/g for CNT, and largely increases to 295 m²/g after coating with NiSiOx, which is less than that of NiSNT (390 m²/g). Although higher specific surface area provides more storage sites for lithium or sodium ions, it might also lead to more surface reactions of electrolyte with electrode, causing larger irreversible capacity. Therefore, a proper specific surface area is desired to increase the ion (Li⁺ or Na⁺) storage sites and enhance the diffusion rate. Based on TGA results of CNT, CNT@NiSiOx and NiSNT (Figure 3d), NiSiOx is ~77.2 wt% in CNT@NiSiOx and stable in a wide range of temperatures. The weight loss may come from the loss of hydrated water in the silicate layers. Its XRD pattern still remains unchanged even after heat treatment at high temperatures (Figure S6), indicating the good thermal stability of CNT@NiSiOx and its potential for high temperature usage.

The porous coaxial CNT@NiSiOx nanocables with tubular

and layered structure are expected to exhibit good electrochemical performance as anode material for lithium ion batteries because of their good electrical conductivity, open layer with large interstitial sites ensuring acceptable Li^+ mobility and accommodating volume variation during Li^+ insertion/extraction. Electrochemical properties of CNT@NiSiOx electrodes are presented in Figure 4. Galvanostatic charge/discharge experiments are carried out at a current density of 50 mA/g (Figure 4a, b). As expected, CNT@NiSiOx exhibits much lower over potential and higher reversible capacity than NiSNT. The first cycle discharge capacity of CNT@NiSiOx reaches 1077 mA h/g and its reversible capacity after 50 cycles is still 489 mA h/g, which is 3.6 times higher than that of NiSNT (107 mA h/g) and substantially higher than other reported values of nickel silicate materials (Table 1).

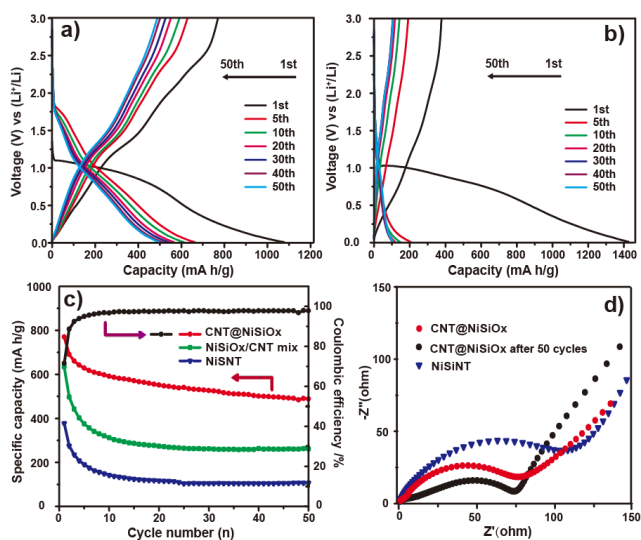


Figure 4. Charge/discharge curves of a) CNT@NiSiOx and b) NiSNT at 1st, 5th, 10th, 20th, 30th, 40th, 50th cycles (current density: 50 mA/g); c) Cycling performance and Coulombic efficiency of CNT@NiSiOx, NiSiOx/CNT mix and NiSNT at current density of 50 mA/g within a voltage window of 0.01-3.0V (vs. Li^+/Li); d) Electrochemical impedance plots of CNT@NiSi, NiSNT and CNT@NiSiOx after 50 cycles.

To confirm the synergistic effect, the mixture of CNT and NiSNT with the same mass ratio as that in CNT@NiSiOx is prepared for comparison. The 50th cycled reversible capacity of CNT@NiSiOx is 87 % higher than that of CNT/NiSNT mixture (Figure 4c), proving that the covalent bonding between NiSiOx and CNT is beneficial for the improvement of lithium storage performance. The cycling performance of CNT is shown in Figure S7. The reversible capacity of CNT is 373 mA h/g. As the percentage of CNT is ~22.8 wt.% in CNT@NiSiOx, the contribution of CNT in terms of capacity could be calculated as 17.4%. The first cycle Coulombic efficiency of CNT@NiSiOx is 71.5%, much higher than those of NiSNT (26.4%) and NiSi/CNT mixture (50.2%), and it reaches nearly 100% in less than 5 cycles. This stable performance might be due to the buffer effect of the one-dimensional structure, the layered structure of NiSiOx nanosheets and the strong C-O-Si covalent bonding during the insertion and extraction of lithium ions.

Table 1. Specific capacities of silicate nanostructures in literatures.

Samples	Morphology	Current density (mA/g)	1 st Coulombic efficiency (%)	1 st charge capacity (mA h/g)	50 th charge capacity (mA h/g)	Ref.
$\text{Ni}_3\text{Si}_2\text{O}_5(\text{OH})_4$	nanotube	20	45.5	693	227*	[32]
$\text{Ni}_3\text{Si}_2\text{O}_5(\text{OH})_4$	nanoflower	20	26.0	428	42	[34]
$\text{Ni}_3\text{Si}_2\text{O}_5(\text{OH})_4/\text{NiO}$	nanoflower	20	47.0	672	126	[34]
NiSNT	nanotube	50	26.4	378	107	This work
NiSiOx/CNT mix	nanotube	50	50.2	634	261	This work
CNT@NiSiOx	nanotube	50	71.5	770	489	This work

* The capacity of 21th cycle.

A major purpose of introducing CNT into CNT@NiSiOx is to improve the electron transfer of NiSiOx since silicate material usually has a poor electrical conductivity. To confirm this effect, EIS measurement is carried out (Figure 4d). The Nyquist plots are constituted by a semicircle at low and medium frequency range and an inclined line at high frequency range. The diameter of the semicircle is related to charge transfer resistance and the inclined line is associated with lithium ion diffusion resistance. The semicircle diameter of CNT@NiSiOx is much smaller than that of NiSNT due to the decreased contact and charge transfer resistances, indicating that CNTs indeed improve the electron diffusion rate in the composite. After charge/discharge for 50 cycles, the charge transfer resistance is further reduced, which may result from the activation of electrode materials during the insertion and extraction of lithium ions.^{66,67}

Rate performance is evaluated from current density of 50 to 1000 mA/g. Fast electron hopping from CNT to NiSiOx nanosheets due to the oxygen bridges ensures better rate performance of CNT@NiSiOx than NiSi/CNT mixture and NiSNT (Figure 5a). Capacities of CNT@NiSiOx retain at 387, 293, 210 and 157 mA h/g at rates of 100, 200, 500 and 1000 mA/g; While capacities of NiSi/CNT mixture are 196, 137, 176 and 41 mA h/g at rates of 100, 200, 500 and 1000 mA/g, respectively. To further confirm the structural stability, the morphology and crystallographic information of CNT@NiSiOx after 50 discharge/charge cycles are analyzed (Figure 5b). Similar XRD patterns of CNT@NiSiOx before (Figure 1d) and after (Figure 5b) charge/discharge for 50 cycles indicates that the crystallography structure remains unchanged. HRTEM images before (Figure 2b) and after (Inset of Figure 5b) further confirm the retained hierarchical morphology. Si 2p XPS profile of CNT@NiSiOx after charge/discharge cycles is also provided in Figure S8, the C-O-Si covalent bond between CNT and NiSiOx nanosheets could still be observed, which proves the structure stability of CNT@NiSiOx during the charge/discharge process.

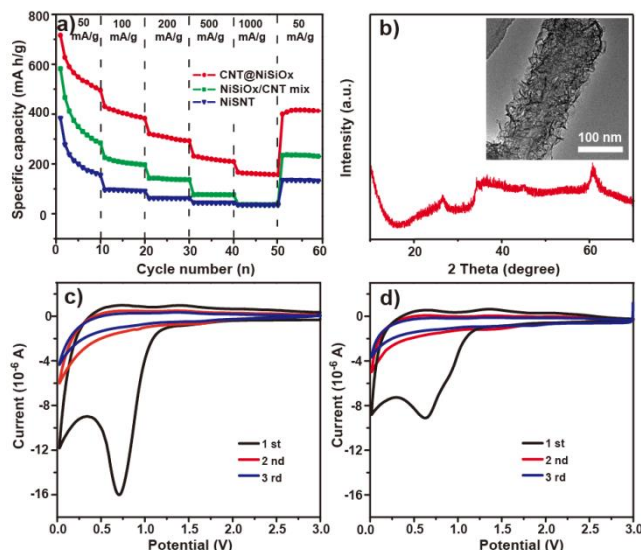


Figure 5. a) Reversible charge capacities of CNT@NiSiOx, NiSiOx/CNT mixture and NiSNT at various rates of 50–1000 mA/g; b) TEM image and XRD spectrum of CNT@NiSiOx after 50 discharge/charge cycles; cyclic voltammograms of c) CNT@NiSiOx and d) NiSNT at 1st, 2nd, 3rd cycles.

In CV profile of CNT@NiSiOx (Figure 5c), a peak at 0.7 V is observed in the first discharge process. However, clear flat platform around 0.7 V in the first discharge curve could not be observed, instead a slope region is present. This is because when anode materials are amorphous or crystals with ultrathin size, the discharge-charge curve usually show slope region, rather than flat plateaus^{65,68–70} (Figure 4a). This peak disappears in the 2nd and 3rd cycles, indicating that it is an irreversible process, most likely due to the formation of solid electrolyte interface (SEI). The formation of SEI is caused by the reaction of electrolyte with electrode. On one hand, it consumes the lithium ions and is responsible for the large irreversible capacity during first cycle, on the other hand, this passivation layer protects the electrode from further dissolution. The same phenomenon is observed in NiSNT electrode. It means that it is NiSiOx component rather than CNT serves as the main active material for lithium storage.

Figure 6a summarizes the contribution of each component of the composite. NiSiOx/CNT mixture exhibits nearly 68 % higher initial specific capacities than NiSNT itself, and 342 mA h/g of the total capacity is ascribed to the effect of CNT. Such a phenomenon is also observed in other reported carbon based composites. However, the capacity of CNT@NiSiOx is about 21% higher than the total sum of the individual capacities of NiSNTs and CNTs, indicating a synergistic effect between these two components. The interlayer spacing and the presence of CNTs stabilize the graphite-like nickel silicate nanosheets throughout the cycling process to accommodate more lithium ions, and keep the active materials electrically interconnected. CNT combined with super-P provides fast electron transport for CNT@NiSiOx to improve the lithium storage property. Therefore, the CNT@NiSiOx electrode exhibits significantly enhanced capacity and cyclability. Nearly a half capacity of CNT@NiSiOx after 50 cycles is ascribed to the synergistic effect (Figure 6a). As a result, lithium ion diffusion and electron transfer are also expedited at high rates for the composites.

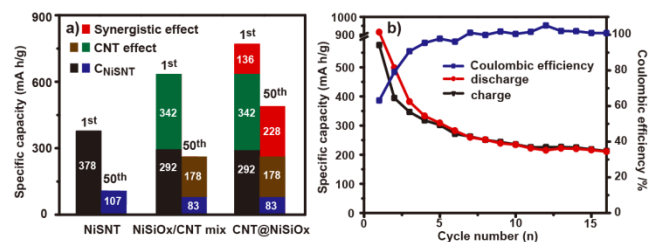


Figure 6. a) The 1st and 50th reversible charge specific capacities of NiSNT, NiSiOx/CNT mixture and CNT@NiSiOx, and the calculated specific capacity based on experimental values; b) Cycling performance and Coulombic efficiency of CNT@NiSiOx at current density of 20 mA/g within a voltage window of 0.01–2.7 V (vs. Na⁺/Na).

Due to the abundant reserves and lower price of Na, SIBs attract lots of attention these years.^{71–75} The storage mechanism of Na in electrode materials is expected to be similar to that of Li. However, most commonly used electrode materials for LIBs are difficult to insert Na⁺ because of its large radius (55 % larger than that of Li⁺).^{4, 76, 77} Thus, developing materials with large interstitial space in the crystallographic structure is an effective method.^{78–80} Because the NiSiOx nanosheets have a large interlayer distance up to 0.74 nm, which is larger than the critical interlayer distance (0.37 nm) for Na⁺ insertion,⁸¹ it may be suitable for sodium storage. Figure 6b shows that the CNT@NiSiOx coaxial nanocable has a high initial charge capacity of 576 mA h/g, and even retains 213 mA h/g at 20 mA/g after 16 cycles. The Coulombic efficiency of CNT@NiSiOx is 63.1% in the first cycle, and then quickly increases to around 100% in less than 5 cycles. There is no reported work about layered silicate used as anode materials for sodium ion batteries yet. Here, we just show its potential application. More detailed characterizations about the storage mechanism of Na are on the way and would be discussed in our further work.

These excellent properties are attributed to the core-shell structure combined layered nickel silicate nanosheets with conductive CNT. First, such a graphite-like layered structure provides massive interlayer spacing for lithium ions or sodium ions transport and storage. Second, NiSiOx nanosheets exposed on the surface of CNT help Li⁺/Na⁺ transport easily between NiSiOx nanosheets and electrolyte. Third, conductive CNT core and C–O–Si covalent bonding effectively improve electron transport in CNT@NiSiOx in comparison to that in NiSiOx/CNT mixture or NiSNT itself. Because of these three advantages, CNT@NiSiOx coaxial nanocable serves as excellent anode material for lithium and sodium storage.

Conclusions

CNT@NiSiOx coaxial nanocables are synthesized using a mild hydrothermal method with CNTs as the hard template and the conductive component. With NiSiOx nanosheets covalently bonded to CNT, CNT@NiSiOx nanocables exhibit good mechanical, thermal and cycling stability. The combination of NiSiOx and CNT shows good synergistic effect by increasing the lithium storage capacity and improving the electron and lithium ion diffusion efficiency of the nanocables. For lithium storage, the charge capacity of CNT@NiSiOx after 50 cycles retains 489

mA h/g at a rate of 50 mA/g, which is 87% higher than that of NiSi/CNT mixture and 3.6 times higher than that of NiSNT alone. The first cycle Coulombic efficiency and rate performance of CNT@NiSiOx are also much better than those of NiSiNT. EIS measurements indicate that the contact and charge transfer resistances of CNT@NiSiOx are much smaller than that of NiSNT because of the covalent bonding between NiSiOx and CNT. The large interlayer spacing allows CNT@NiSiOx to be intercalated by not only lithium ions but also sodium ions with larger diameters. For sodium storage, the coaxial nanocables show a high initial charge capacity of 576 mA h/g, and even retain a charge capacity of 213 mA h/g at 20 mA/g after 16 cycles. The CNT@NiSiOx coaxial nanocables show large potential in the application as anode materials for lithium ions or sodium ions batteries.

Acknowledgements

Financial support from the National Natural Science Foundation of China (51402012, 51125010), the Fundamental Research Funds for the Central Universities (YS201402), and the State Key Laboratory of Organic-Inorganic Composites (201404) is gratefully acknowledged.

Notes and references

State Key Laboratory of Organic-Inorganic Composites, College of Materials Science and Engineering, Beijing University of Chemical Technology, Beijing 100029, China

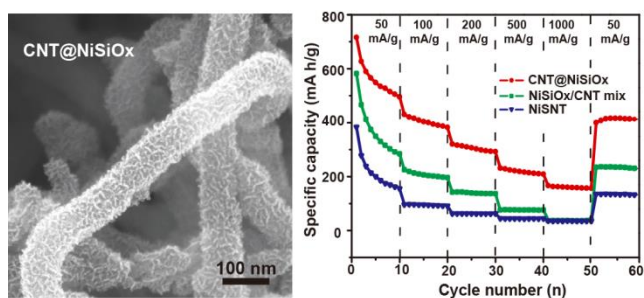
*Corresponding author. Tel/Fax: +86-10-64428582. E-mail: qujin@mail.buct.edu.cn (J. Qu), yuzz@mail.buct.edu.cn (Z.-Z. Yu)

† Electronic Supplementary Information (ESI) available: [SEM image of carbon nanotubes; SEM images of CNT@NiSiOx and NiSNT synthesized at different times; SEM image and XRD patterns of CNT@NiSiOx after calcinated at different temperatures.]. See DOI: 10.1039/b000000/x/

- J. M. Tarascon and M. Armand, *Nature*, 2001, **414**, 359-367.
- A. S. Arico, P. Bruce, B. Scrosati, J. M. Tarascon and W. Van Schalkwijk, *Nat. Mater.*, 2005, **4**, 366-377.
- M. J. Armstrong, C. O'Dwyer, W. J. Macklin and J. D. Holmes, *Nano Res.*, 2014, **7**, 1-62.
- Y. Sun, L. Zhao, H. Pan, X. Lu, L. Gu, Y. S. Hu, H. Li, M. Armand, Y. Ikuhara, L. Chen and X. Huang, *Nat. Commun.*, 2013, **4**, 1870.
- N. Yabuuchi, M. Kajiyama, J. Iwatate, H. Nishikawa, S. Hitomi, R. Okuyama, R. Usui, Y. Yamada and S. Komaba, *Nat. Mater.*, 2012, **11**, 512-517.
- Q. An, F. Xiong, Q. Wei, J. Sheng, L. He, D. Ma, Y. Yao and L. Mai, *Adv. Energy Mater.*, 2015, **5**, 1401963.
- J. B. Goodenough and Y. Kim, *J. Power Sources*, 2011, **196**, 6688-6694.
- J. B. Goodenough and K. S. Park, *J. Am. Chem. Soc.*, 2013, **135**, 1167-1176.
- V. Etacheri, R. Marom, R. Elazari, G. Salitra and D. Aurbach, *Energy Environ. Sci.*, 2011, **4**, 3243-3262.
- L. Dai, D. W. Chang, J.-B. Baek and W. Lu, *Small*, 2012, **8**, 1130-1166.
- S. Han, D. Wu, S. Li, F. Zhang and X. Feng, *Small*, 2013, **9**, 1173-1187.
- M. V. Reddy, G. V. S. Rao and B. V. R. Chowdari, *Chem. Rev.*, 2013, **113**, 5364-5457.
- J. S. Chen and X. W. Lou, *Small*, 2013, **9**, 1877-1893.
- M. Ge, X. Fang, J. Rong and C. Zhou, *Nanotechnology*, 2013, **24**, 422001.
- X. Huang, Z. Zeng and H. Zhang, *Chem. Soc. Rev.*, 2013, **42**, 1934-1946.
- B. Wang, X. Li, B. Luo, X. Zhang, Y. Shang, A. Cao and L. Zhi, *ACS Appl. Mater. Interfaces*, 2013, **5**, 6467-6472.
- X. Li and L. Zhi, *Nanoscale*, 2013, **5**, 8864-8873.
- Y. X. Wang, S. L. Chou, H. K. Liu and S. X. Dou, *Carbon*, 2013, **57**, 202-208.
- K. Tang, L. Fu, R. J. White, L. Yu, M. M. Titirici, M. Antonietti and J. Maier, *Adv. Energy Mater.*, 2012, **2**, 873-877.
- J. Cabana, L. Monconduit, D. Larcher and M. Rosa Palacin, *Adv. Mater.*, 2010, **22**, E170-E192.
- L. Ji, Z. Lin, M. Alcoutlabi and X. Zhang, *Energy Environ. Sci.*, 2011, **4**, 2682-2699.
- H. Li, Z. Wang, L. Chen and X. Huang, *Adv. Mater.*, 2009, **21**, 4593-4607.
- A. Manthiram, A. V. Murugan, A. Sarkar and T. Muraliganth, *Energy Environ. Sci.*, 2008, **1**, 621-638.
- M. Rosa Palacin, *Chem. Soc. Rev.*, 2009, **38**, 2565-2575.
- B. Scrosati and J. Garche, *J. Power Sources*, 2010, **195**, 2419-2430.
- Y. Yang, Y. Zhuang, Y. He, B. Bai and X. Wang, *Nano Res.*, 2010, **3**, 581-593.
- J. Qu, W. Li, C. Y. Cao, X. J. Yin, L. Zhao, J. Bai, Z. Qin and W. G. Song, *J. Mater. Chem.*, 2012, **22**, 17222-17226.
- J. Qu, C. Y. Cao, Y. L. Hong, C. Q. Chen, P. P. Zhu, W. G. Song and Z. Y. Wu, *J. Mater. Chem.*, 2012, **22**, 3562-3567.
- C. X. Gui, Q. Q. Wang, S. M. Hao, J. Qu, P. P. Huang, C. Y. Cao, W. G. Song and Z. Z. Yu, *ACS Appl. Mater. Interfaces*, 2014, **6**, 14653-14659.
- S. Zhang, W. Xu, M. Zeng, J. Li, J. Li, J. Xu and X. Wang, *J. Mater. Chem. A*, 2013, **1**, 11691-11697.
- A. Corma, *Chem. Rev.*, 1997, **97**, 2373-2419.
- X. Wang, J. Zhuang, J. Chen, K. B. Zhou and Y. D. Li, *Angew. Chem., Int. Ed.*, 2004, **43**, 2017-2020.
- J. Wu, Y. J. Zhu, S. W. Cao and F. Chen, *Adv. Mater.*, 2010, **22**, 749-753.
- Q. Fang, S. Xuan, W. Jiang and X. Gong, *Adv. Funct. Mater.*, 2011, **21**, 1902-1909.
- R. C. Longo, K. C. Santosh and K. Cho, *J. Electrochem. Soc.*, 2014, **161**, A1461-A1467.
- Y. Yang, Q. Liang, J. Li, Y. Zhuang, Y. He, B. Bai and X. Wang, *Nano Res.*, 2011, **4**, 882-890.
- J. Qu, Y. Yan, Y. X. Yin, Y. G. Guo and W. G. Song, *ACS Appl. Mater. Interfaces*, 2013, **5**, 5777-5782.
- Y. Yang, R. Jin, S. Song and Y. Xing, *Mater. Lett.*, 2013, **93**, 5-8.
- I. Quinzeni, S. Ferrari, E. Quartarone, D. Capsoni, M. Caputo, A. Goldoni, P. Mustarelli and M. Bini, *J. Power Sources*, 2014, **266**, 179-185.
- B. J. Landi, M. J. Ganter, C. D. Cress, R. A. DiLeo and R. P. Raffaele, *Energy Environ. Sci.*, 2009, **2**, 638-654.
- C. de las Casas and W. Li, *J. Power Sources*, 2012, **208**, 74-85.

42. S. Goriparti, E. Miele, F. De Angelis, E. Di Fabrizio, R. P. Zaccaria and C. Capiglia, *J. Power Sources*, 2014, **257**, 421-443.
43. F. F. Cao, Y. G. Guo, S. F. Zheng, X. L. Wu, L. Y. Jiang, R. R. Bi, L. J. Wan and J. Maier, *Chem. Mater.*, 2010, **22**, 1908-1914.
44. C. K. Chan, H. Peng, G. Liu, K. McIlwrath, X. F. Zhang, R. A. Huggins and Y. Cui, *Nat. Nanotechnol.*, 2008, **3**, 31-35.
45. Y. Wu, Y. Wei, J. Wang, K. Jiang and S. Fan, *Nano Lett.*, 2013, **13**, 818-823.
46. A. L. M. Reddy, M. M. Shaijumon, S. R. Gowda and P. M. Ajayan, *Nano Lett.*, 2009, **9**, 1002-1006.
47. Y. Gu, F. Wu and Y. Wang, *Adv. Funct. Mater.*, 2013, **23**, 893-899.
48. L. Xue, G. Xu, Y. Li, S. Li, K. Fu, Q. Shi and X. Zhang, *ACS Appl. Mater. Interfaces*, 2013, **5**, 21-25.
49. G. Cui, L. Gu, L. Zhi, N. Kaskhedikar, P. A. van Aken, K. Muellen and J. Maier, *Adv. Mater.*, 2008, **20**, 3079-3083.
50. H. X. Zhang, C. Feng, Y. C. Zhai, K. L. Jiang, Q. Q. Li and S. S. Fan, *Adv. Mater.*, 2009, **21**, 2299-+.
51. K. Bindumadhavan, S. K. Srivastava and S. Mahanty, *Chem. Commun.*, 2013, **49**, 1823-1825.
52. T. H. Yoon and Y. J. Park, *Solid State Ionics*, 2012, **225**, 498-501.
53. A. Varzi, C. Tauerbert, M. Wohlfahrt-Mehrens, M. Kreis and W. Schuetz, *J. Power Sources*, 2011, **196**, 3303-3309.
54. Z. An, L. He, M. Toda, G. Yamamoto, T. Hashida and T. Ono, *Nanotechnology*, 2015, **26**, 195601.
55. T. Zhu, H. B. Wu, Y. Wang, R. Xu and X. W. Lou, *Adv. Energy Mater.*, 2012, **2**, 1497-1502.
56. H. B. Li, M. H. Yu, F. X. Wang, P. Liu, Y. Liang, J. Xiao, C. X. Wang, Y. X. Tong and G. W. Yang, *Nat. Commun.*, 2013, **4**.
57. L. Xu, Y. S. Ding, C. H. Chen, L. Zhao, C. Rinkus, R. Joesten and L. Suib, *Chem. Mater.*, 2008, **20**, 308-316.
58. I. M. Ali, Y. H. Kotp and I. M. El-Naggar, *Desalination*, 2010, **259**, 228-234.
59. C. Wan and B. Chen, *Nanoscale*, 2011, **3**, 693-700.
60. M. C. Hsiao, C. C. M. Ma, J. C. Chiang, K. K. Ho, T. Y. Chou, X. Xie, C. H. Tsai, L. H. Chang and C. K. Hsieh, *Nanoscale*, 2013, **5**, 5863-5871.
61. G. S. Li, L. P. Li, R. L. Smith and H. Inomata, *Journal of Molecular Structure*, 2001, **560**, 87-93.
62. D. Pan, S. Wang, B. Zhao, M. Wu, H. Zhang, Y. Wang and Z. Jiao, *Chem. Mater.*, 2009, **21**, 3136-3142.
63. J. Qu, Y. X. Yin, Y. Q. Wang, Y. Yan, Y. G. Guo and W. G. Song, *ACS Appl. Mater. Interfaces*, 2013, **5**, 3932-3936.
64. G. Zhou, D. W. Wang, L. C. Yin, N. Li, F. Li and H. M. Cheng, *ACS Nano*, 2012, **6**, 3214-3223.
65. J. S. Cho, Y. J. Hong and Y. C. Kang, *ACS Nano*, 2015, **9**, 4026-4035.
66. Z. Cai, L. Xu, M. Yan, C. Han, L. He, K. M. Hercule, C. Niu, Z. Yuan, W. Xu, L. Qu, K. Zhao and L. Mai, *Nano Lett.*, 2015, **15**, 738-744.
67. Y. Sun, X. Hu, W. Luo, F. Xia and Y. Huang, *Adv. Funct. Mater.*, 2013, **23**, 2436-2444.
68. Y. Xu, G. Jian, Y. Liu, Y. Zhu, M. R. Zachariah and C. Wang, *Nano Energy*, 2014, **3**, 26-35.
69. Y. Yin, Y. Hu, P. Wu, H. Zhang and C. Cai, *Chem. Commun.*, 2012, **48**, 2137-2139.
70. Y. Liu, Y. Xu, X. Han, C. Pellegrinelli, Y. Zhu, H. Zhu, J. Wan, A. C. Chung, O. Vaaland, C. Wang and L. Hu, *Nano Lett.*, 2012, **12**, 5664-5668.
71. S. Y. Hong, Y. Kim, Y. Park, A. Choi, N.-S. Choi and K. T. Lee, *Energy Environ. Sci.*, 2013, **6**, 2067-2081.
72. M. D. Slater, D. Kim, E. Lee and C. S. Johnson, *Adv. Funct. Mater.*, 2013, **23**, 947-958.
73. J. Jiang, Y. Li, J. Liu, X. Huang, C. Yuan and X. W. Lou, *Adv. Mater.*, 2012, **24**, 5166-5180.
74. V. Palomares, P. Serras, I. Villaluenga, K. B. Hueso, J. Carretero-Gonzalez and T. Rojo, *Energy Environ. Sci.*, 2012, **5**, 5884-5901.
75. H. Pan, Y. S. Hu and L. Chen, *Energy Environ. Sci.*, 2013, **6**, 2338-2360.
76. Z. Jian, W. Han, X. Lu, H. Yang, Y. S. Hu, J. Zhou, Z. Zhou, J. Li, W. Chen, D. Chen and L. Chen, *Adv. Energy Mater.*, 2013, **3**, 156-160.
77. L. Wang, Y. Lu, J. Liu, M. Xu, J. Cheng, D. Zhang and J. B. Goodenough, *Angew. Chem., Int. Ed.*, 2013, **52**, 1964-1967.
78. Y. You, X. L. Wu, Y. X. Yin and Y. G. Guo, *Energy Environ. Sci.*, 2014, **7**, 1643-1647.
79. Y. You, X. L. Wu, Y. X. Yin and Y. G. Guo, *J. Mater. Chem. A*, 2013, **1**, 14061-14065.
80. Y. U. Park, D. H. Seo, H. S. Kwon, B. Kim, J. Kim, H. Kim, I. Kim, H. I. Yoo and K. Kang, *J. Am. Chem. Soc.*, 2013, **135**, 13870-13878.
81. Y. Cao, L. Xiao, M. L. Sushko, W. Wang, B. Schwenzer, J. Xiao, Z. Nie, L. V. Saraf, Z. Yang and J. Liu, *Nano Lett.*, 2012, **12**, 3783-3787.

TOC



5 Carbon nanotube@layered nickel silicate (CNT@NiSiO_x) coaxial nanocables with flexible nickel silicate nanosheets grown on conductive carbon nanotubes (CNTs) are synthesized by a mild hydrothermal method. Massive interlayer space for lithium
10 or sodium storage, improved electrical conductivity and C-O-Si covalent bonding are benefit for structure stability during discharge/charge cycles and enhanced electrochemical property.